




Influence of fast neutron irradiation on the phase composition and optical properties of homogeneous SiO_x and composite Si–SiO_x thin films

Diana Nesheva¹, Zsolt Fogarassy², Margit Fabian², Temenuga Hristova-Vasileva¹, Attila Sulyok², Irina Bineva¹, Evgenia Valcheva³, Krassimira Antonova¹, and Peter Petrik^{2,*} 

¹Institute of Solid State Physics, Bulgarian Academy of Sciences, 72 Tzarigradsko Chaussee Blvd., 1784 Sofia, Bulgaria

²Centre for Energy Research, Konkoly Thege Miklos ut 29-33, 1121 Budapest, Hungary

³Faculty of Physics, Sofia University 'St. Kliment Ohridski', 5 James Bourchier, Blvd., 1164 Sofia, Bulgaria

Received: 25 June 2020

Accepted: 12 September 2020

Published online:
26 October 2020

© Springer Science+Business
Media, LLC, part of Springer
Nature 2020

ABSTRACT

Layers and devices utilizing semiconductor nanocrystals have been the subjects of intensive research due to applications in opto- and microelectronic devices, solar cells, detectors, memories and in many more fields. We have shown previously that those nanocrystals in dielectric matrices undergo a substantial reformation during electron irradiation. The research of the interaction between semiconductor nanoclusters and irradiation is important for both the intentional modification of the structures and for understanding the stability of those devices under harsh, radiative conditions (e.g. space, nuclear, medical diagnosis, or similar applications). In the present research, we investigated the influence of neutron irradiation on substoichiometric silicon oxide. We investigated both homogeneous case and inhomogeneous case of matrices with silicon nanoclusters. We found that a fast neutron flux of 5.5×10^{13} neutrons/cm² s and a fluence of 3.96×10^{17} neutrons/cm² induce phase separation in the homogeneous films, whereas it decreases the volume fraction of the amorphous silicon phase caused by the reducing size of amorphous nanoclusters in the inhomogeneous films.

Handling Editor: Kevin Jones.

Address correspondence to E-mail: petrik@mfa.kfki.hu

<https://doi.org/10.1007/s10853-020-05338-3>

Introduction

Nanosized silicon crystals and amorphous nanoclusters, embedded in wide-gap insulating matrices, have shown significant promises for application in optoelectronics and solar cells [1–5]. Applications in nanoelectronics as charge trapping non-volatile memories based on the floating gate concept [6] and resistive random-access memories [7, 8] have also been proposed. Metal–oxide–semiconductor (MOS) structures with Ge and Si nanocrystals have been considered for inclusion in dosimeters of ionizing radiation [9–12] and in photodetectors of visible and ultraviolet light [13–16]. The devices using metal–oxide–silicon structures with Si nanoparticles are beneficial because they are compatible with Si-based microfabrication technology.

Devices with nanocrystals could be used in fields where a more or less high degree of radiation tolerance is required: space and avionic applications, nuclear power plants, medical diagnostic imaging and therapy, material processing, etc. When operated in such environments, they may be directly struck by photons, electrons, protons, neutrons, or heavier particles which may alter their electrical properties and disturb their operation. Therefore, understanding the properties of amorphous and crystalline nanoclusters and their behavior under extreme conditions is important for both fundamental research and the future development of materials and devices with high degree of radiation tolerance [17].

It is expected that materials and devices with nanoparticles would have better resistance to ionizing radiation. The nanoparticles play an important role in both maintaining the mechanical strength by pinning dislocations and enhancing radiation tolerance by providing extra sinks for irradiation-induced point defects. Indeed, irradiation experiments with high energy protons and high fluencies, as well as experiments with gamma radiation, have shown that the radiation hardness of non-volatile memory devices with Si nanocrystals is much better than the hardness of standard floating gate memories [6, 18].

Neutrons have no charge and react primarily with the nucleus, causing transmutation (conversion of one chemical element into its other isotope or into another chemical element) or displacement of lattice

atoms. Many publications have reported results on the influence of fast neutrons that have strong displacement effect [19] on the radiation hardness of nanostructured ferritic alloys for nuclear reactors [20, 21]. Attention has also been addressed to the effect of heavy neutron irradiation of crystalline and amorphous SiO₂ materials [22] used in communication technologies (as optical fibers, thin films for electrical insulation, optical lenses for excimer laser lithography, etc.), as well as to the effects of high neutron fluences (10^{17} and 10^{18} neutrons/cm², $E > 0.1$ MeV) on silica glasses (KU1, KS-4V and I301) [23]. The neutron irradiation-induced structural changes result in an increase in the number of strained bonds and formation of new defects that alter the optical properties of the glasses. It has been reported that neutron irradiation of amorphous nanoparticles from SiO₂ with size of 20 nm by a flux of 2×10^{13} neutrons/cm² s for up to 20 h did not cause crystallization but particles of larger size (70 nm) appeared [24].

The number of papers on the effects of fast neutron irradiation of composites with semiconductor nanoparticles is quite limited. It has been reported that fast neutron irradiation of Ge nanocrystals embedded in an amorphous SiO₂ matrix at a neutron fluence of 10^{20} neutrons/cm² leads to partial destruction and amorphization of the Ge nanocrystals [25]. Recently, ensembles of Si nanocrystals with the size of 100 nm have been neutron-irradiated with a flux of 2×10^{13} neutrons/(cm²s) for 20 h and nanocrystal agglomeration has been observed [26]. We found reports neither on the effect of fast neutron irradiation of amorphous or crystalline Si nanoparticles embedded in an amorphous SiO_x ($x \leq 2$) matrix (composite Si–SiO_x films), nor about neutron-induced Si nanoparticle growth in silicon-enriched silicon oxide films.

In this paper, we are concerned with the responses of homogeneous silicon-rich silicon oxide films and composite Si–SiO_x films exposed to fast neutron irradiation. The changes in the surface roughness and phase composition of both kinds of films are investigated by several complementary characterization techniques, and the results obtained are explained assuming neutron irradiation-induced phase separation and amorphous nanocluster size decrease.

Experimental details

Sample preparation

Silicon suboxide (SiO_x) layers with oxygen content of $x = 1.2$ and thicknesses in the range of 280–300 nm were prepared by thermal evaporation of silicon monoxide (SiO) at a vacuum of 1×10^{-3} Pa and deposition rate of 5 nm/s [27]. The films were deposited on chemically cleaned n-type (100) crystalline silicon substrates, maintained at room temperature. The deposition rate and film thickness were controlled by a preliminary calibrated quartz crystal microbalance system. To ensure film stability at ambient conditions, all specimens with as-deposited films were furnace annealed at 250 °C for 30 min in argon atmosphere. Previous investigations showed [28] that the films annealed at 250 °C were homogeneous and these films form the group of homogeneous samples investigated here (denoted by ‘ SiO_x ’—see Fig. 1). In addition, two groups of composite films were prepared by thermal annealing of some homogeneous films at 700 °C or 1000 °C in nitrogen atmosphere for 60 min (‘a-Si- SiO_x ’ and ‘nc-Si- SiO_x ’ in Fig. 1, respectively). Infrared transmission investigations on the annealed films revealed an increase in the oxygen content in the films, thus indicating that an annealing-induced phase separation took place [27]. High-temperature annealing of Si-rich oxide films in an inert atmosphere is frequently used

in order to grow amorphous or crystalline silicon nanoclusters [1, 8]. High-resolution transmission electron microscopy (HRTEM) and electron diffraction are applied for obtaining direct evidences for the existence of crystalline Si clusters/particles (called “silicon nanocrystals”). Areas with crystalline structure in an amorphous oxide matrix and crystal fringes are observed in the macrographs and diffraction patterns, respectively. Since the structure of amorphous nanoclusters does not differ from the structure of the amorphous matrix, the standard HRTEM and electron diffraction do not reveal amorphous nanoclusters. Therefore, Raman scattering is frequently used which provides a fast and non-destructive way to determine whether silicon nanoclusters are amorphous or crystalline [8]. Our previous HRTEM and Raman scattering investigations have revealed that upon annealing of homogeneous SiO_x films at 1000 °C Si nanocrystals (nc-Si) in a SiO_2 matrix were grown (nc-Si- SiO_2 composite films) [28, 29], while the annealing at 700 °C caused formation of amorphous Si (a-Si) nanoclusters in a SiO_x matrix [27, 28] (a-Si- SiO_x composite films, $x_{\text{matrix}} = 1.7\text{--}1.8$ [30, 31]). Since we had obtained reproducible results for the formation of Si nanocrystals upon thermal annealing of our SiO_x films at 1000 °C [18, 32, 33], in this study we have not carried out HRTEM measurements and adopted that Si nanocrystals exist in the films annealed at 1000 °C with size of around 4–6 nm.

Samples from each group were neutron-irradiated in the Budapest Research Reactor using fast neutron channel Nr. 47/2, where the fast neutron flux (energy range > 200 keV) was $\Phi_f = 5.5 \times 10^{13}$ neutrons/ (cm^2s) ; the neutron fluence was 3.96×10^{17} neutrons/ cm^2 . The samples were irradiated for 2 h. The samples were packed in high-purity Al foil (99.9995% from Alfa Aesar, $d = 0.038$ mm), and the monitor foils from inside to out were Zr (0.025 mm foil, Alfa Aesar), Au (0.1% Au in 0.1 mm Al foil, IRMM-530) and Fe (0.1 mm, EC-NMR524) [34]. For a schematic graph of the sample preparations and notations, see Fig. 1.

Sample characterization

High-resolution transmission electron microscopy (HRTEM) investigations were carried out in an aberration corrected THEMIS microscope at 200 keV. For energy-dispersive spectroscopy (EDS) mapping, a super-X detector was used. Cross-sectional TEM

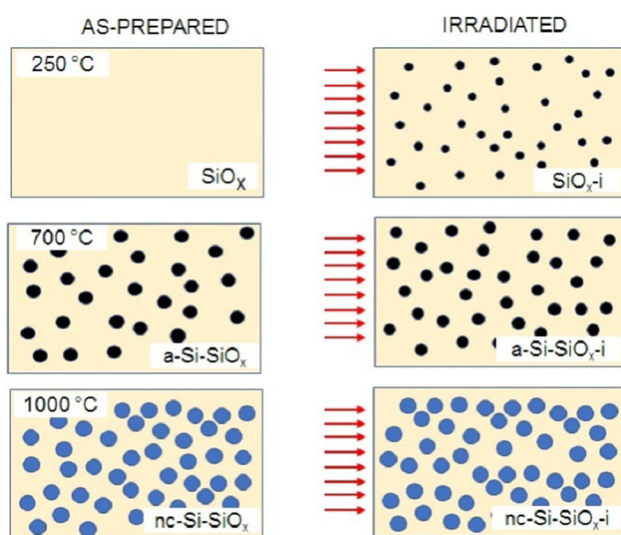


Figure 1 Schematic representation of the preparation and naming of the samples. Amorphous and crystalline nanoclusters are represented by black and blue dots, respectively.

samples were prepared by conventional Ar ion beam milling. Electron diffraction (ED) patterns were measured in a CM-20 TEM, operated at 200 keV.

X-ray photoelectron spectroscopy (XPS) analysis was carried out on non-irradiated and neutron-irradiated a-Si-SiO_x composite films. It was conducted under ultrahigh vacuum conditions (2×10^{-7} Pa). The samples were exposed to 70 °C heat treatment for 48 h, which is the standard baking procedure of the applied vacuum system. The photoelectron spectra were obtained using X-ray radiation (Al anode with water cooling, 15 keV excitation). The XPS measurement yielded information of the average surface composition of an area of ca. 5 mm diameter. Constant energy resolution of 1.5 eV was provided by a special cylindrical mirror analyzer with retarding field (type DESA 150, Staib Instruments Ltd.). All spectra were recorded with 0.1 eV energy steps, and the O 1s (532 eV); C 1s (285 eV); Si 2s (150 eV); and Si 2p (100 eV) lines were detected. Spectra were evaluated by applying the usual Shirley-background subtraction. Peak intensities were derived by Gaussian-Lorentzian fitting for the peak shapes that provides a decomposition of the complex Si shape for subpeaks. Elemental compositions were calculated from subpeak areas assuming homogeneous model. Sensitivity factors were calculated from the area of reference spectra in Ref. [35].

Multiple-angle spectroscopic ellipsometry (SE) measurements were performed which ensure a good accuracy in finding the proper structural model to describe the real structure of the samples. The SE measurements were carried out on Woollam's automatic spectroscopic ellipsometer M2000DI working in the reflection mode in the wavelength range of 350–1000 nm for films annealed at 250 °C and 700 °C and 250–1000 nm for films annealed at 1000 °C; three angles of incidence (55°, 60° and 65°) were used. The obtained data were further fitted by applying the Cody-Lorentz model [36] and the model based on the Bruggeman effective medium approximation (B-EMA) [37, 38] that is the most frequently used model for the evaluation of composite samples. The Woollam's CompleteEASE program with the Cody-Lorentz oscillator parameterization was applied to homogeneous films/matrices.

Fourier transform infrared (FTIR) transmission measurements in normal incidence geometry were used to evaluate the composition of the homogeneous SiO_x films as well as the composition of the matrices

of composite films. A Bruker Vertex 70 instrument was used operated in the spectral region of 1500–400 cm⁻¹ with a resolution of 1 cm⁻¹. Raman scattering measurements were also performed to get information about the pure silicon phase in the non-irradiated and neutron-irradiated homogeneous and composite films. The measurements were carried out on a HORIBA Jobin Yvon Labram HR 800 spectrometer and excitation with a He-Ne (633 nm) laser is applied. The laser beam with 1 mW power was focused on a spot of about 1 μm in diameter, and the spectral resolution was 1 cm⁻¹ or better.

Atomic force microscopy (AFM) measurements were carried out to investigate the effect of the neutron irradiation on the surface roughness of all groups of films. A Multimode V microscope (Bruker, ex. Veeco, Santa Barbara, CA) was used for the experiments. Imaging was performed in tapping mode with scan rate 0.7 Hz, and the images resolution was 512 lines per scan direction (l/s.d.). Aluminum-coated silicon cantilevers TAP150-AI-G (Budget Sensors Innovative Solutions Bulgaria Ltd.) with resonant frequency of 150 kHz and spring constant of 5 N/m were used. Images were just flattened, and no further processing was performed. The image analysis was done by means of Nanoscope 7.30 on an area of 5 μm × 5 μm.

Results and discussion

Two-dimensional AFM surface image of a non-irradiated homogeneous SiO_x film is shown in Fig. 2a. The film surface looks very smooth, and the root mean square roughness determined is $R_{\text{q,n}} = 0.55$ nm (Table 1). The surface images of the films annealed at $T_a = 700$ °C and 1000 °C are very similar. The results in Table 1 show that the surface roughness of the composite films is up to 40% smaller than that of the SiO_x films and a tendency of surface roughness reduction is observed with increasing annealing temperature. This observation is in line with our previous results reported for films with initial composition of $x = 1.1$ and 1.3 [39]. Annealing-induced roughness decrease has been also reported for SiO_x films prepared by various techniques—thermal evaporation of silicon powder [40], reactive sputtering [41] and LPCVD [42]. High-temperature annealing is applied to achieve atomically smooth surfaces on silicon [43–45], and this approach is based mostly

Figure 2 Two-dimensional AFM surface images of non-irradiated (a) and neutron-irradiated (b) homogeneous SiO_x films.

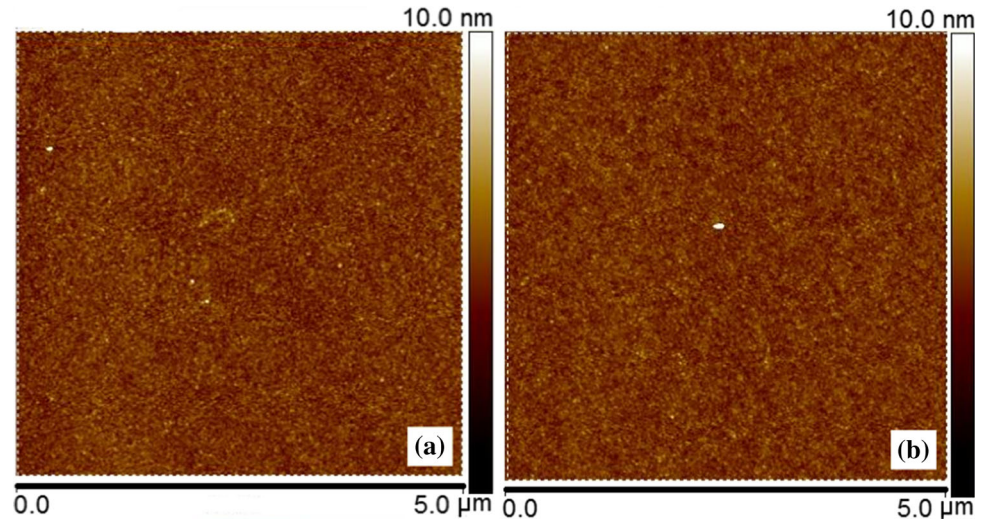


Table 1 Root mean square surface roughness of non-irradiated and neutron-irradiated samples

Sample type	Roughness (nm)	
	Non-irradiated	Neutron-irradiated
SiO_x	0.55	0.57
a-Si-SiO _x	0.47	0.45
nc-Si-SiO ₂	0.31	0.35

on surface self-diffusion. Probably surface self-diffusion is the main reason for the annealing-induced roughness decrease we observed. The very good surface smoothness of the homogeneous SiO_x films and the annealing-induced roughness decrease taking place together with the growth of silicon nanoparticles are important for incorporation of the composite films in memory devices, UV detectors, or dosimeters for ionizing radiation [11, 18, 46, 47]. Figure 2b shows two-dimensional surface image of a neutron-irradiated homogeneous SiO_x film. One can see that the neutron irradiation did not significantly affect the film surface (Table 1). Similar results have been obtained for the films annealed at $T_a = 700$ °C and $T_a = 1000$ °C (Table 1). The conclusion is that the neutron irradiation did not cause appreciable changes of the surface roughness.

Any radiation, in particular fast neutrons, causing damage in the bulk of a material also causes displacement of surface atoms, as well as sputtering, i.e., the release of atoms at the surface. For neutrons, the sputtering yield, defined as the mean number of atoms removed from the surface per incident

neutron, is generally of the order of 10^{-5} atoms per neutron [17, 48, 49]. At a fluence of 10^{17} neutrons/cm², the released atoms could be roughly 10^{12} atoms/cm², i.e., no effective surface sputtering may be expected. On the other hand, the energy deposited in the surface layer could facilitate the surface self-diffusion thus keeping the very good surface smoothness.

FTIR transmission measurements were carried out to investigate the phase separation induced by thermal annealing and neutron irradiation, as well as the effect of the neutron irradiation on the pure silicon phase in the annealed films. Conclusions were drawn by analyzing the behavior of the asymmetric stretching band which is related to vibration of the Si–O–Si bridge. For stoichiometric SiO_2 , this band has a minimum at around 1080 cm⁻¹ [50] and consists of one transverse optical (TO) mode peaked at ≈ 1080 cm⁻¹ and longitudinal optical (LO) modes in the range of 1200 – 1300 cm⁻¹ (LO shoulder). When the oxygen content in SiO_x films is less than stoichiometric ($x < 2$) the minimum of the stretching band is shifted to the low frequencies (“red” shift), the LO shoulder disappears and the full width at half minimum of the band increases due to an increase in the lattice disorder [27, 50, 51]. IR transmittance spectra of non-irradiated SiO_x films annealed at 250 °C, 700 °C and 1000 °C are shown in Fig. 3. It is seen from the figure that the band minimum of the film annealed at 250 °C is situated at 991 cm⁻¹, which, according to the established relation between the position of the band minimum and the oxygen content in our silicon oxide films [30, 31], gives

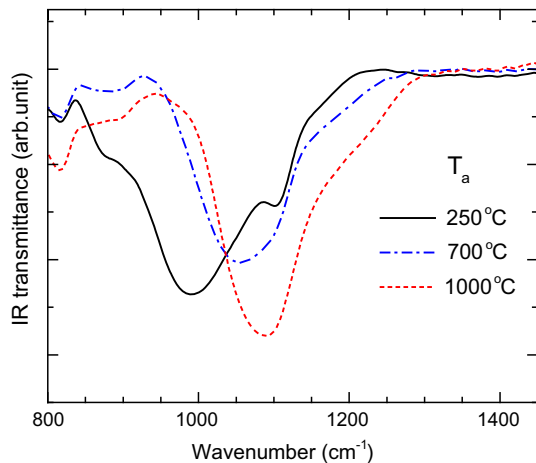


Figure 3 FTIR spectra of a non-irradiated homogeneous SiO_x film annealed at 250 °C and two non-irradiated composite films prepared by thermal annealing at 700 °C and 1000 °C.

$x \approx 1.2$ for the homogeneous film investigated here. Upon thermal annealing, the band is “blue”-shifted to 1056 cm^{-1} in the spectrum of the film annealed at 700 °C and to 1089 cm^{-1} in the spectrum of the film annealed at 1000 °C. The observed “blue” shifts indicate that in the film annealed at 700 °C an incomplete phase separation took place ($x_{\text{matrix}} = 1.7\text{--}1.8$) and complete phase separation occurred in the film annealed at 1000 °C ($x_{\text{matrix}} = 2$). Previously reported results have shown that pure amorphous silicon phase is formed in the films thermally annealed at 700 °C, while the annealing at 1000 °C results in the formation of isolated randomly distributed Si nanocrystals [28, 52]. The average size of Si nanocrystals is of 3–5 nm in films with initial $x = 1.3$ and 4–6 nm in films with $x = 1.15$ [18, 32, 33].

Figure 4 compares the IR transmittance spectra of non-irradiated and neutron-irradiated films. A significant “blue” shift of the stretching band from 991 cm^{-1} to 1025 cm^{-1} is seen in Fig. 4a. The band in the spectrum of the a-Si-SiO_x film (Fig. 4b) shows a small “red” shift (of around 7 cm^{-1}). In the nc-Si-SiO₂ film the shape of the band is not appreciably changed, and the band shows a very small “red” shift (of around 2 cm^{-1}) (Fig. 4c). The “blue” shift in Fig. 4a can be connected with phase separation (and formation of pure Si phase) in the homogeneous samples caused by the neutron irradiation. Using the relation in Refs. [30] and [31], the estimated oxygen content in the matrix of the irradiated SiO_x sample is $x_{\text{matrix}} \approx 1.5$ and one can expect that the amount of the pure Si phase is less than that in the a-Si-SiO_x films ($x_{\text{matrix}} = 1.7\text{--}1.8$).

The small “red” shift of the stretching band upon neutron irradiation seen in Fig. 4b could be related to slight decrease in the oxygen content in the matrix. This may happen if Si atoms from the existing pure amorphous silicon phase formed during the thermal annealing procedure return back to the matrix which results in a decrease in the size of a-Si nanoclusters [52]. Results from the XPS and SE investigations described below give further evidences of this assumption. The very similar shape of the bands in Fig. 4c implies that no appreciable changes in the lattice order of the SiO₂ matrix took place upon neutron irradiation of the nc-Si-SiO₂ films and the very small “red” shift of the band implies that the Si nanocrystals have better resistance against fast neutron irradiation than the amorphous nanoclusters.

As mentioned in Sect. 2.1 of Experimental details, multiple previous HRTEM investigations on the films

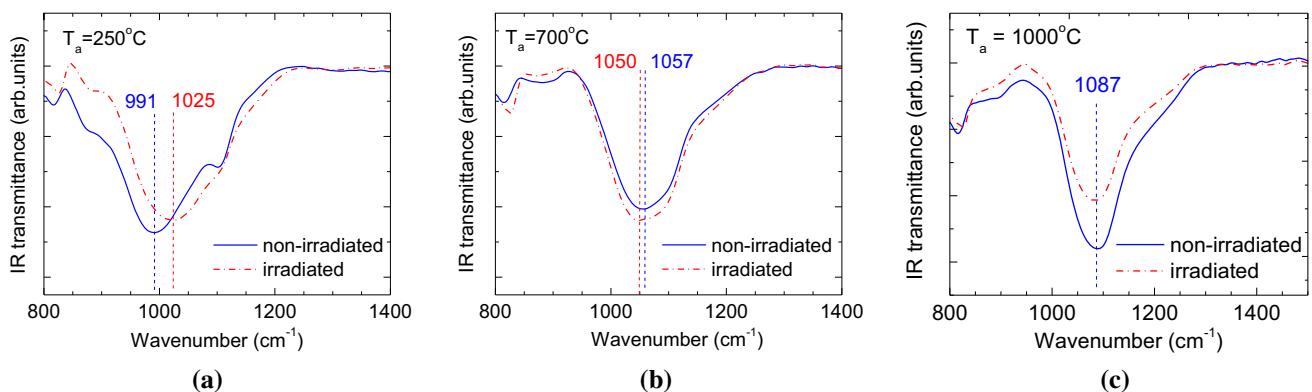
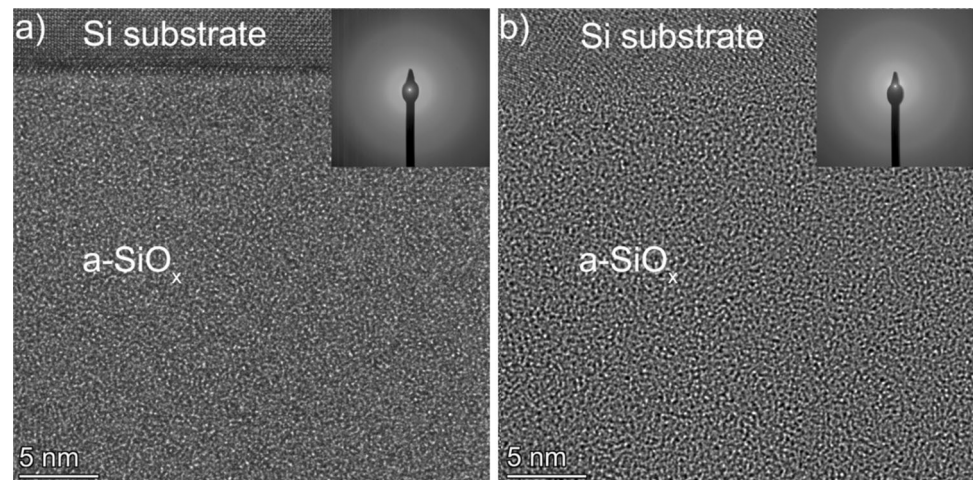


Figure 4 Comparison of FTIR spectra of non-irradiated and neutron-irradiated homogeneous SiO_x film (a), a-Si-SiO_x composite film (b) and nc-Si-SiO₂ composite film (c).

Figure 5 HRTEM images and SAED patterns of non-irradiated (a) and neutron-irradiated (b) SiO_x films annealed at 700 °C. The inset shows the nanobeam diffraction patterns of the non-irradiated and irradiated samples.



annealed at 1000 °C have proven formation of Si nanocrystals with the size of around 4–6 nm. In this study, HRTEM measurements were carried out on homogeneous SiO_x films and films annealed at 700 °C in which the IR transmission results showed well-expressed neutron irradiation-induced changes. HRTEM images of non-irradiated and neutron-irradiated films annealed at 700 °C are shown in Fig. 5. The evaluated local layer thicknesses based on the TEM images are in the range 230–300 nm. Figure 5, as well as the figures obtained for the homogeneous films, shows that all four samples are completely amorphous. No crystalline Si phase has been detected. The EDS maps have not revealed a-Si nanoclusters since a rather small cluster size is expected (around 2 nm [53]). Due to the overlaps of the nanoclusters on thick parts of the TEM samples and because of the surface oxidation on the thin parts of the TEM samples, these small clusters cannot be detected with the EDS measurements.

X-ray photoelectron spectroscopy (XPS) measurements were carried out to get more information about the material phases of non-irradiated and neutron-irradiated a-Si-SiO_x films annealed at 700 °C. Due to the small information depth (≈ 3 nm) of XPS, the spectroscopy detects its signal from the surface region. Because of air exposure of the specimens, their surface is oxidized to SiO_2 and contaminated. To obtain information from the bulk, the surface region had been removed by ion sputtering. Practically, longer depth profiles were measured by applying ion sputtering and spectra detection alternately which showed the distribution of components with increasing depth. The sputtering speed and the total

depth were estimated on the basis of our earlier measurements. The depth profiles showed a slow change of the film composition with increasing depth and stabilization after about 40 nm. Therefore, we regarded this as reaching the bulk composition. The silicon peak showed chemical changes with increasing depth from the single SiO_2 state (at the surface) to the triple state $\text{Si}(\text{O}_2)\text{-Si}(\text{O})\text{-Si}$. Although both the Si2s and Si2p lines show the oxidation state of the silicon, in case of the 2p line the difference is larger; thus, it was used for quantitative evaluation.

The 2p line curves of a non-irradiated and a neutron-irradiated film annealed at 700 °C are shown in Fig. 6a. It is clearly seen that neutron irradiation changes the curve shape indicating a change in the composition. To make a quantitative evaluation of the film composition, the curves were decomposed into three subpeaks (see Fig. 6b, c) that are associated with three oxidation states of the Si atoms: (i) elemental Si detected at binding energy of ≈ 100 eV; (ii) SiO_x ($x \approx 1$) detected at binding energy of ≈ 101.9 eV and (iii) SiO_2 detected at binding energy of ≈ 103.1 eV. (The ‘ SiO_2 ’ notation means Si atoms in SiO_2 state.) The compositions obtained are given in Table 2, and they show that both the non-irradiated and the neutron-irradiated films have elemental Si, i.e., pure Si phase (nanoclusters) which is in line with our previous conclusions [18]. The irradiated film has less elemental Si and SiO_2 and more SiO_x than the non-irradiated one. Thus, XPS investigations show that the neutron irradiation of the films annealed at 700 °C influenced their chemical composition in such a way that both elemental Si and SiO_2 were transformed to SiO_x keeping the total atomic composition.

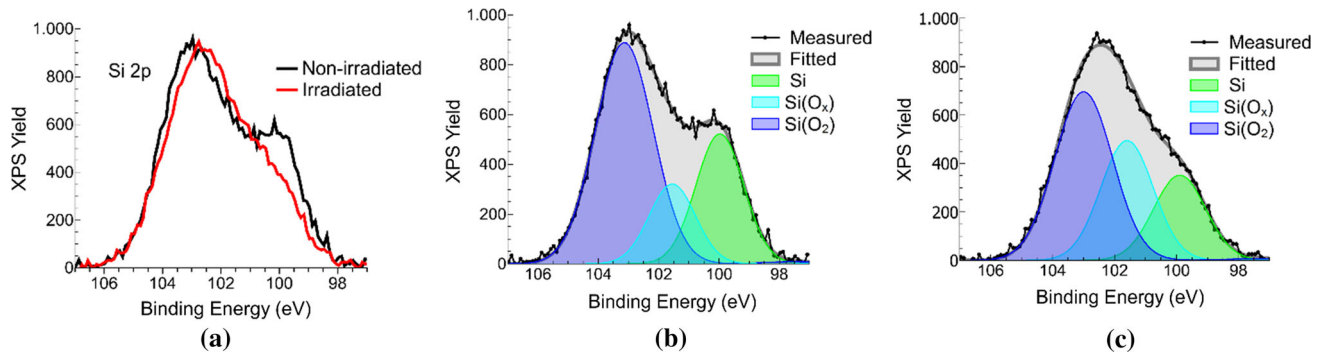


Figure 6 Comparison of XPS spectra observed on the non-irradiated and irradiated samples annealed at 700 °C **(a)**. Decomposition of the spectra in **a** are also shown for both of the non-irradiated **(b)** and irradiated **(c)** samples. The three bands of

decomposition are associated with three oxidation states of the Si atoms: elemental Si at binding energy of ≈ 100 eV; SiO_x ($x \approx 1$) at binding energy of ≈ 101.9 eV; and SiO_2 at binding energy of ≈ 103.1 eV.

Table 2 Composition of a non-irradiated and a neutron-irradiated a-Si– SiO_x film

	O	$\text{Si}(\text{O}_2)$ at. %	$\text{Si}(\text{O}_x)$ at. %	Si at. %
Non-irradiated	54.7	25.6	7.3	12.3
Irradiated	53.3	22.3	14.3	10.1

This observation is in agreement with the IR transmission result (the “red” band shift in Fig. 4b), and it can be explained assuming that the neutron irradiation caused bond breaks thus reducing some SiO_2 to SiO_x and the free oxygen released found its way to the elemental Si by forming SiO_x . The reduction of the elemental Si could be due to some decrease in the a-Si nanocluster size and/or to complete disappearance of the smallest nanoclusters.

Raman scattering spectra of non-irradiated and neutron-irradiated homogeneous and a-Si– SiO_x films,

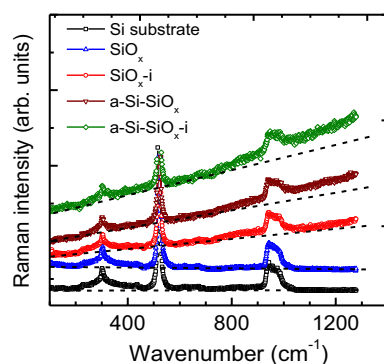


Figure 7 Raman scattering spectra of non-irradiated and neutron-irradiated homogeneous (annealed at 250 °C) and a-Si– SiO_x composite (annealed at 700 °C) films.

as well as of a crystalline silicon substrate, are shown in Fig. 7. No well-expressed changes in the shape and position of the Raman bands are seen, but one can notice the existence of background in the spectra of neutron-irradiated homogeneous film and both non-irradiated and neutron-irradiated a-Si– SiO_x composite films; the background increases with the wavenumber. As known, three-dimensional crystalline Si is an indirect-band semiconductor and its photoluminescence (PL) at room temperature is of very low intensity. However, the amorphous and crystalline silicon nanoclusters with a size of a few nanometers show an intense PL due to carrier confinement [54]. We have also reported room temperature photoluminescence from a(nc)Si– SiO_x composite films [28]. In some a-Si– SiO_x , it was visible with a naked eye and its intensity increased with decreasing nanocluster size [55]. The background observed in Fig. 7 is most likely due to PL from a-Si nanoclusters. As expected, no PL background is observed in the spectra of the Si substrates and non-irradiated homogeneous film, while such background is seen in the other three spectra. The appearance of PL background in the spectrum of the neutron-irradiated homogeneous film indicates that a-Si nanoclusters were formed upon neutron irradiation. The PL from these nanoclusters is of lower intensity than that from the a-Si clusters in non-irradiated a-Si– SiO_x composite films which implies that the amount of the pure Si phase in the irradiated homogeneous films is less than in the films annealed at 700 °C. These observations are in very good agreement with the IR transmission results.

Figure 7 shows that the neutron irradiation of a-Si-SiO_x films causes some PL intensity increase which can be due to the increase in the amount of pure silicon phase or to some decrease in the nanocluster size. Keeping in mind that the IR transmission and XPS results have shown that upon neutron irradiation the amount of pure silicon phase decreases, one can relate the increase in the PL background to a certain decrease in the nanocluster size.

SE was also applied in order to get quantitative information about the neutron irradiation changes in phase composition of homogeneous and composite films. SE is a sensitive method for the investigation of semiconductor and dielectric nanostructures [56, 57 and references therein]. The native SiO₂ was not removed from the surface of the c-Si substrates before the deposition of the oxide layers, and therefore, it was taken into account in the fitting procedure with a thickness of 2 nm [52]. Best results in the fitting procedure were obtained assuming that the homogeneous/composite layers consist of two sublayers—sublayer 1 with thickness *d*₁ situated on the native oxide and top sublayer 2 with thickness *d*₂. The data for the composition of sublayer 2 of all samples, as well as for the composition of sublayer 1 of all composite films and the neutron-irradiated homogeneous film, were obtained by applying the B-EMA. From the SE data, the influence of the nanoparticle content on sublayer 1 was specified as the effective refractive index of the layer. The obtained results are summarized in Table 3.

It is seen from Table 3 that sublayer 2 in the films has a higher oxygen content than sublayer 1, which confirms the XPS results showing that the surface is postdeposition-oxidized during the stay of the films

in air. The thickness of sublayer 2 in the homogeneous films is greater than that in the a-Si-SiO_x composite films as neutron irradiation does not change appreciably the thickness of sublayer 2. The smaller thickness of sublayer 2 in the films annealed at 700 °C can be related to film densification taking place upon high-temperature annealing [27]. One can also see from Table 3 that both thermal annealing at 700 °C and neutron irradiation of homogeneous films increase significantly the oxygen content of sublayer 2; the thermally induced increase is greater than that caused by the irradiation. By analogy with sublayer 1 in which thermal annealing at 700 °C causes *x*-increase from 1.2 to 1.7–1.8, the observed increase in the oxygen content in sublayer 2 can be related to annealing/neutron irradiation-induced phase separation. Keeping in mind the IR transmission results for layer 1 (Fig. 4a, b), it is not surprising that the oxygen increase in sublayer 2 caused by the neutron irradiation is weaker (51.6% SiO₂) than the annealing-induced one (69.8% SiO₂).

The SE data in Table 3 for the volume fraction (*f*) of the pure Si phase in sublayer 1 show that the neutron irradiation of homogeneous films results in the appearance of pure Si phase of *f* = 2.4%. The a-Si phase in non-irradiated a-Si-SiO_x films is *f* = 8.0%, and it decreases to *f* = 6.6% upon neutron irradiation. In the non-irradiated nc-Si-SiO₂ films, predominantly crystalline Si phase of *f*_c = 20.7% but also a-Si phase of *f*_a = 4.0% has been detected (*f* = *f*_c + *f*_a = 24.7%). The neutron-induced changes of both phases in the nc-Si-SiO₂ films are negligible (*f* = *f*_c + *f*_a = 24.5%). Computer simulations of the IR transmission spectra of a(nc)Si-SiO_x (*x* ≤ 2) composite films were performed in Ref. [31], and the values of the volume

Table 3 Annealing temperature (*T*_a), sublayer thickness (*d*₁, *d*₂), amount and crystallinity of the pure Si phase and effective refractive index at 632.8 nm of sublayer 1 (*n*₁) of non-irradiated and neutron-irradiated films obtained from SE measurements. Volume fraction data

<i>T</i> _a	Non-irradiated films					Neutron-irradiated films				
	<i>d</i> ₁ (nm)	<i>d</i> ₂ (nm)	Layer 1 Pure Si phase %	Layer 2 SiO ₂ %	<i>n</i> ₁	<i>d</i> ₁ (nm)	<i>d</i> ₂ (nm)	Layer 1 Pure Si phase %	Layer 2 SiO ₂ %	<i>n</i> ₁
250 °C	241	68	–	21.4	1.791	233.5	69.7	2.4% of a-Si	51.6	1.744
700 °C	247	34	8.0% a-Si (20%)	69.8	1.959	246	36	6.6% of a-Si	72.4	1.934
1000 °C	288	6	20.7% of nc-Si 4.0% of a-Si (27%)	–	1.945	289	6	20.2% of nc-Si 4.3% of a-Si	–	1.942

of the Si phase from Ref. [31] are shown in parentheses for 700 °C and 1000 °C. Errors of thicknesses, volume fractions and refractive indices are less than a few nanometers, 1% and 10⁻³, respectively

fractions at which good correspondence of the simulated and experimental IR transmission spectra was observed are given in Table 3. It is seen that the volume fraction in the a-Si-SiO_x films obtained by SE is much smaller than the *f*-value from Ref. [31], while in the nc-Si-SiO₂ films both values are quite similar. We discussed in Ref. [52] that very small Si nanoclusters cannot be distinguished by the light as a separate phase. The average size of a-Si nanoclusters grown at 700 °C (~ 2 nm) is significantly smaller than the average size of nanocrystals (4–5 nm). The similarity of the c-Si volume fraction in the nc-Si-SiO₂ films determined from the SE and IR transmission results indicates that most likely only a part of a-Si clusters are too small and not distinguished by the light as a separate phase. One can think that in the a-Si-SiO_x films more than a half of the nanoclusters are rather small and not distinguished by the light and hence it can be suggested that the pure silicon volume fraction in the neutron-irradiated homogeneous films is higher than 2.4%; based on the above estimated *x* = 1.5 in the matrix one could expect a value as high as *f* ≈ 0.15.

It is seen from Table 3 that the neutron irradiation causes certain decrease in the effective refractive index. Dispersion curves for the effective refractive index (*n*) of non-irradiated and neutron-irradiated films are displayed in Fig. 8. Upon neutron irradiation, the refractive index of homogeneous film significantly decreases, in the a-Si-SiO_x film *n* also decreases though not so much, and *n* shows a very small decrease in the nc-Si-SiO₂ film. The refractive

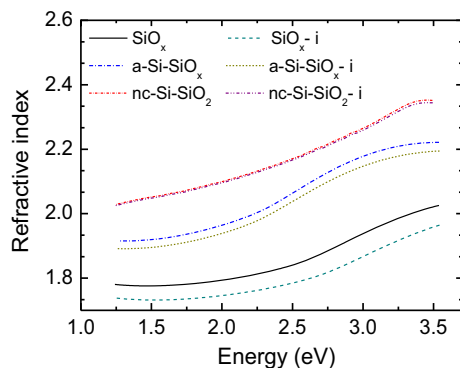


Figure 8 Dispersion curves of the effective refractive index of non-irradiated and neutron-irradiated homogeneous SiO_x films (annealed at 250 °C) and composite films containing amorphous Si nanoclusters (annealed at 700 °C) and Si nanocrystals (annealed at 1000 °C). The curves of the films annealed at 1000 °C are shifted up for clarity.

index of SiO_x films depends on their composition as *n* decreases with increasing oxygen content *x* [50, 58]. The considerable *n*-decrease in the homogeneous films can be understood taking into account the above assumptions that the neutron irradiation causes phase separation, formation of a-Si nanoclusters and considerable increase in the oxygen content of the matrix (from *x* = 1.2 to *x* = 1.5). The observed *n* decrease upon neutron irradiation of the a-Si-SiO_x film can be related to the reduction of the pure a-Si phase from *f* = 0.08 to *f* = 0.062 (Table 3). The result is in agreement with the XPS data and supports the idea for neutron-induced decrease in the a-Si nanocluster size. The dispersion curves of the refractive index of non-irradiated and neutron-irradiated nc-Si-SiO₂ films are very close to each other (Fig. 8). This result, together with the marginal variations in the film phase composition (Table 2) and the very small change in the position (of ≈ 2 cm⁻¹) and shape of the stretching band in the IR transmission spectra (Fig. 4c), implies that the changes of the pure silicon phase in these films caused by the neutron irradiation applied are fairly weak.

It should be mentioned that the phase separation in the homogeneous films and a-Si nanocluster size decrease in a-Si-SiO_x films have also been observed upon irradiation with fast electrons (20 MeV, fluence of 3.6 × 10¹⁵ electrons/cm²) [52]. A comparison of the FTIR results shows that the fast neutron irradiation causes stronger phase separation than the irradiation with fast electrons; the “blue” shift of the stretching band in the FTIR spectra of neutron-irradiated film is around 34 cm⁻¹, while in the electron irradiated film it is only 3 cm⁻¹ [59]. This could be expected keeping in mind that the neutrons react primarily with the nucleus, causing displacement of lattice atoms. The observed *n* decrease (and a-Si nanocluster size decrease) caused by both the neutron and electron irradiation is well expressed and a bit larger in the case of neutron irradiation. It is interesting that the fast electron irradiation with a fluence of 3.6 × 10¹⁵ electrons/cm² results in a bit higher *n* decrease [59] than that observed upon neutron irradiation (Fig. 8), but the results show that the changes in the composite nc-Si-SiO₂ films caused by fast neutrons and electrons are weak, i.e., these films demonstrate a high radiation resistance. The high radiation resistance and the preserved layer smoothness are of great importance for development and application of devices with Si nanocrystals, such as UV and photodetectors [1, 3, 11, 14], dosimeters [18], non-

volatile memories [6, 8, 18] and solar cells [1, 3, 5], which operate in neutron radiation environment in nuclear power stations, aviation and cosmos. The underlying mechanism of high radiation resistance of an alloy containing amorphous and nanocrystalline phases of the same composition has been explored in a recent study [60]. The investigation of the microstructural evolution under neutron irradiation shows that such materials demonstrate excellent resistance to neutron irradiation which is due to the rapid and full annihilation of irradiation-induced vacancies in the nanocrystal regions and systematic self-recovering of free volumes in the amorphous matrix.

Conclusions

Homogeneous SiO_x ($x = 1.2$) and a(nc)-Si- SiO_x composite films containing amorphous Si nanoclusters/Si nanocrystals were irradiated by fast neutrons at a fluence of 3.96×10^{17} neutrons/cm². An analysis of the effect of neutron irradiation on the films properties was made based on XPS, HRTEM, AFM, IR transmission, SE and Raman scattering results. It has been found that the applied fluence of the neutron irradiation does not cause appreciable damage of the film surface which remains very smooth. The irradiation causes phase separation in the homogeneous films resulting in an increase in the oxygen content from $x = 1.2$ in the non-irradiated film to $x \approx 1.5$ in the matrix of the irradiated one and formation of pure amorphous silicon phase of considerable volume fraction ($f \approx 0.15$). It has also been concluded that upon neutron irradiation the volume fraction of the pure a-Si phase in a-Si- SiO_x composite films decreases due to a decrease in the size of amorphous Si nanoclusters and the oxygen content in the matrix decreases. This has been explained assuming that the neutron irradiation caused bond breaks thus reducing some SiO_2 to SiO_x and the free oxygen released reduced the Si nanocluster size by forming SiO_x . The films with Si nanocrystals have shown a high radiation resistance.

Acknowledgements

We would like to thank K. Gmeling for performing neutron irradiation of the samples. P. Petrik is grateful for support from the OTKA K131515 project. The Bulgarian co-authors thank the European

Regional Development Fund, Ministry of Economy of Bulgaria, Operational Programme “Development of the Competitiveness of the Bulgarian economy” 2007–2013, Contract No BG161PO003-1.2.04-0027-C0001, for purchasing the Bruker Vertex 70 spectrophotometer.

References

- [1] Pavese L, Turan R (eds) (2010) Silicon nanocrystals fundamentals, synthesis and applications. Wiley, Germany, p 652. ISBN: 978-3-527-32160-51
- [2] Greben M, Khoroshyy P, Liu X, Pi X, Valenta J (2017) Fully radiative relaxation of silicon nanocrystals in colloidal ensemble revealed by advanced treatment of decay kinetics. *J Appl Phys* 122:034304. <https://doi.org/10.1063/1.4993584>
- [3] Ni Z, Zhou S, Zhao S, Peng W, Yang D, Pi X (2019) Silicon nanocrystals: unfading silicon materials for optoelectronics. *Mater Sci Eng R* 138:85–117
- [4] Conibeer G (2012) Si and other group IV quantum dot based materials for tandem solar cells. *Energy Procedia* 15:200–205
- [5] Schnabel M, Weiss C, Löper P, Wilshaw PR, Janz S (2015) Self-assembled silicon nanocrystal arrays for photovoltaics. *Phys Stat Solidi (a)* 212:1649–1661
- [6] Verrelli E, Tsoukalas D (2011) Radiation hardness of flash and nanoparticle memories. In: Stievano I (ed) Flash memories, in radiation hardness of flash and nanoparticle memories, in flash memories. InTech and references therein. ISBN: 978-953-307-272-2
- [7] Gismatulin AA, Kruchinin VN, Gritsenko VA, Prosvirin IP, Yen T-J, Chin A (2019) Charge transport mechanism of high-resistive state in RRAM based on SiO_x . *Appl Phys Lett* 114:033503
- [8] Volodin V, Gritsenko V, Gismatulin A, Chin A (2019) Silicon nanocrystals and amorphous nanoclusters in SiO_x and SiN_x : atomic, electronic structure, and memristor effects. In: Movahedi B (ed) Nanocrystalline materials. IntechOpen
- [9] Aktag A, Yilmaz E, Mogaddam NA, Aygun G, Cantas A, Turan R (2010) Ge nanocrystals embedded in SiO_2 in MOS based radiation sensors. *Nucl Instr Meth B* 268:3417
- [10] Nedev N, Manolov E, Nesheva D, Krezhov K, Nedev R, Curiel M, Valdez B, Mladenov A, Levi Z (2012) Metal-oxide-semiconductor structures containing silicon nanocrystals for application in radiation dosimeters. *Sens Lett* 10:833
- [11] Nesheva D, Nedev N, Curiel M, Dzhurkov V, Arias A, Manolov E, Mateos D, Valdez B, Bineva I, Herrera R (2015) Application of metal-oxide-semiconductor structures

- containing silicon nanocrystals in radiation dosimetry. *Open Phys* 13:63
- [12] Slav A, Lepadatu AM, Stavarache I, Dascalescu I, Maraloiu AV, Negriela C, Logofatu C, Stoica T, Teodorescu VS, Ciurea ML, Lazanu S (2019) Orthorhombic HfO₂ with embedded Ge nanoparticles in nonvolatile memories used for the detection of ionizing radiation. *Nanotechnology* 30:445501
- [13] Shieh J-M, Lai Y-F, Ni W-X, Kuo H-C, Fang C-Y, Huang JY, Pan C-L (2007) Orthorhombic HfO₂ with embedded Ge nanoparticles in nonvolatile memories used for the detection of ionizing radiation. *Appl Phys Lett* 90:051105
- [14] Yu Z, Aceves-Mijares M (2009) A ultraviolet-visible-near infrared photodetector using nanocrystalline Si superlattice. *Appl Phys Lett* 95:081101
- [15] Hossain SM, Anopchenko A, Prezioso S, Ferraioli L, Pavesi L, Pucker G, Bellutti P, Binetti S, Acciarri M (2008) Sub-band gap photoresponse of nanocrystalline silicon in a metal-oxide-semiconductor device. *J Appl Phys* 104:074917
- [16] Curiel M, Nedev N, Paz J, Perez O, Valdez B, Mateos D, Arias A, Nesheva D, Manolov E, Nedev R, Dzurkov V (2019) UV Sensitivity of MOS structures with silicon nanoclusters. *Sensors* 19:2277
- [17] Sobolev NA (2008) In: Henini M (ed) *Handbook of self assembled semiconductor nanostructures for novel devices in photonics and electronics*. Elsevier Inc., Academic Press chapter 13. ISBN: 978-0-08-046325-4
- [18] Nesheva D, Nedev N, Curiel M, Bineva I, Valdez B and Manolov E, *Silicon Oxide Films Containing Amorphous or Crystalline Silicon Nanodots for Device Applications*, in *Quantum Dots – A Variety of New Applications* Ameenah A-A editor InTech, 2012, chapter 9, 183-206. ISBN: 978-953-51-0483-4
- [19] Spieler H (1997) *Introduction to radiation-resistant semiconductor devices and circuits*. AIP Conf Proc 390:1–31
- [20] Odette GR, Alinger MJ, Wirth BD (2008) Recent developments in irradiation-resistant steels. *Annu Rev Mater Res* 38:471–503
- [21] Liu X, Miao Y, Wu Y, Maloy SA, Stubbins JF (2017) Stability of nanoclusters in an oxide dispersion strengthened alloy under neutron irradiation. *Scripta Mater* 138:57–61
- [22] Awazu K, Kawazoe H (2003) Strained Si–O–Si bonds in amorphous SiO₂ materials: a family member of active centers in radio, photo, and chemical responses. *J Appl Phys* 94:6243–6262
- [23] León M, Giacomazzi L, Girard S, Richard N, Martín P, Martín-Samos L, Ibarra A, BoukenterOuerdane AY (2014) Neutron irradiation effects on the structural properties of KU1, KS-4V and I301 silica glasses. *IEEE Trans Nucl Sci* 61:1522–1530
- [24] Huseynov E, Garibov A, Mehdiyeva R (2016) TEM and SEM study of nano SiO₂ particles exposed to influence of neutron flux. *J Mater Res Technol* 5:213–218
- [25] Levy Sh, Shlimak I, Dressler DH, Grinblat J, Gofer Y, Lu T, Ionov AN (2011) Structure and Spatial Distribution of Ge Nanocrystals Subjected to Fast Neutron Irradiation. *Nanomater Nanotechnol* 1:52–57
- [26] Garibli A, Garibov AA, Huseynov EM (2019) Defect formation processes in the silicon nanoparticles under the neutron irradiation. *Mod Phys Lett B* 33:1950315
- [27] Nesheva D, Bineva I, Levi Z, Aneva Z, Merdzhanova T, Pivin JC (2003) Composition, structure and annealing-induced phase separation in SiO_x films produced by thermal evaporation of SiO in vacuum. *Vacuum* 68:1
- [28] Nesheva D, Raptis C, Perakis A, Bineva I, Aneva Z, Levi Z, Alexandrova S, Hofmeister H (2002) Raman scattering and photoluminescence from Si nanoparticles in annealed SiO_x thin films. *J Appl Phys* 92:4678–4683
- [29] Curiel MA, Nedev N, Nesheva D, Soares J, Haasch R, Sardela M, Valdez B, Sankaran B, Manolov E, Bineva I, Petrov I (2010) Microstructural characterization of thin SiO_x films obtained by physical vapor deposition. *Mat Sci Eng B* 174:132–136
- [30] Bineva I (2004) *Silicon nanoparticles in thermal SiO_x thin films*. PhD thesis, Sofia, Bulgaria
- [31] Donchev V, Nesheva D, Todorova D, Germanova K, Valcheva E (2012) Characterization of Si–SiO_x nanocomposite layers by comparative analysis of computer simulated and experimental infra-red transmission spectra. *Thin Solid Films* 520:2085
- [32] Mateos D, Arias A, Nedev N, Curiel M, Dzhurkov V, Manolov E, Nesheva D, Contreras O, Valdez B, Bineva I, Raymond O, Siqueiros JM (2013) Metal–oxide–semiconductor structures with two and three-region gate dielectric containing silicon nanocrystals: structural infrared and electrical properties. *NSTI-Nanotech* 2013(1):396–399
- [33] Mateos D, Curiel M, Nedev N, Nesheva D, Machorro R, Manolov E, Abundiz N, Arias A, Contreras O, Valdez B, Raymond O, Siqueiros JM (2013) TEM and spectroscopic ellipsometry studies of multilayer gate dielectrics containing crystalline or amorphous Si nanoclusters. *Physica E* 51:111–114
- [34] Szentmiklosi L, Parkanyi D, Sziklai-Laszlo I (2016) Upgrade of the Budapest neutron activation analysis laboratory. *J Radional Nucl Chem* 309:91–99
- [35] Vincent Crist B (2000) *Handbook of Monochromatic XPS spectra*. Wiley, Hoboken
- [36] Ferlauto AS, Ferreira GM, Pearce JM, Wronski CW, Collins RW (2002) Analytical model for the optical functions of amorphous semiconductors from the near-infrared to

- ultraviolet: Applications in thin film photovoltaics. *J Appl Phys* 92:2424
- [37] Amans D, Callard S, Ganarie A, Joseph J, Ledoux G, Huisken F (2003) Ellipsometric study of silicon nanocrystal optical constants. *J Appl Phys* 93:4173
- [38] Lohner T, Szekeres A, Nikolova T, Vlaiikova E, Petrik P, Huhn G, Havancsak K, Lisovskyy I, Zlobin S, Indutnyy IZ, Shepeliavyy PE (2009) Optical models for ellipsometric characterization of high temperature annealed nanostructured SiO₂ films. *J Optoelect Adv Mater* 11:1288
- [39] Curiel M, Petrov I, Nedev N, Nesheva D, Sardela M, Murata Y, Valdez B, Manolov E, Bineva I (2010) Formation of Si nanocrystals in their SiO₂ films for memory device application. *Mater Sci Forum Special vol AFM-NANOMAT* 664:101–104
- [40] Evtukh A, Hartnagel H, Yilmazoglu O, Mimura H, Pavlidis D (2015) Vacuum nanoelectronic devices: novel electron sources and applications. John Wiley & Sons Ltd, Chichester, p 209
- [41] Alarcón-Salazar J, Aceves-Mijares M, Roman-López S, Falcony C (2012) Characterization and fabrication of SiO_x nano-metric films, obtained by reactive sputtering. In: *Proceedings 9th international conference on electrical engineering, computing science and automatic control (CCE)*, Mexico City, pp 1–5.
- [42] Luna-López JA, Morales-Sánchez A, Aceves-Mijares M, Yu Z, Domínguez C (2009) Analysis of surface roughness and its relationship with photoluminescence properties of silicon-rich oxide films. *J Vac Sci Technol, A* 27:57
- [43] Kolari K, Vehmas T, Svensk O, Törmä P, Aalto T (2010) Smoothing of microfabricated silicon features by thermal annealing in reducing or inert atmospheres. *Phys Scr* 2010:014017
- [44] Acosta-Alba PE, Kononchuk O, Gourdel Ch, Claverie A (2014) Surface self-diffusion of silicon during high temperature annealing. *J Appl Phys* 115:134903
- [45] Araki K, Takeda R, Sudo H, Izunome K, Zhaokolari X (2014) *J Surf Eng Mater Adv Technol* 4:249–256
- [46] Manolov E, Nedev N, Dzhurkov V, Nesheva D, Paz-Delgadillo J, Curiel-Alvarez M, Valdez-Salas B (2019) Investigation of resistive switching in SiO₂ layers with Si nanocrystals. *J Phys Conf Ser* 1186:012022
- [47] Curiel M, Nedev N, Paz J, Perez O, Valdez B, Mateos D, Arias A, Nesheva D, Manolov E, Nedev R, Dzhurkov V (2019) UV sensitivity of MOS structures with silicon nanoclusters. *Sensors* 19:2277
- [48] Behrisch R (1982) Sputtering with neutrons. *J Nucl Mater* 108–109:73–82
- [49] Bang-jiao YE, Yang-mei FAN, Kasuga Y, Ikeda Y, Zhou X-Y, Han R-D (1999) Reduced sputtering yields induced by fast neutrons. *Chin Phys Lett* 16:844–846
- [50] Tsu DV, Lucovsky G, Davidson BN (1989) Effects of the nearest neighbors and the alloy matrix on SiH stretching vibrations in the amorphous SiO_r: H (0<r<2) alloy system. *Phys Rev B* 40:1795
- [51] Tomozeiu N (2011) Silicon oxide (SiO_x, 0<x<2): a challenging material for optoelectronics. In: Predeep P (ed) *Optoelectronics—materials and techniques*. InTech, Rijeka. ISBN: 978-953-307-276-0
- [52] Hristova-Vasileva T, Petrik P, Nesheva D, Fogarassy Z, Lábár J, Kaschieva S, Dmitriev SN, Antonova K (2018) Influence of 20 MeV electron irradiation on the optical properties and phase composition of SiO_x thin films. *J Appl Phys* 123:195303
- [53] Nesheva D, Nedev N, Levi Z, Brüggemann R, Manolov E, Kirilov K, Meier S (2008) Absorption and transport properties of Si rich oxide layers annealed at various temperatures. *Semicond Sci Technol* 23:045015
- [54] Ischenko AA, Fetisov GV, Aslalnov LA (2015) Nanosilicon: properties, synthesis, applications, methods of analysis and control. CRC Press, Taylor and Francis Group ss, Boca Raton, pp 1–3
- [55] Bineva I, Nesheva D, Šćepanović M, Grujić-Brojčin M, Popović ZV, Levi Z (2007) Dependence of photoluminescence from a-Si nanoparticles on the annealing time and exciting wavelength. *J Luminescence* 126:7–13
- [56] Petrik P, Lohner T, Fried M, Gyulai J, Boell U, Berger R, Lehnert W (2002) Ellipsometric study of the polysilicon/thin oxide/single-crystalline silicon structure and its change upon annealing. *J Appl Phys* 92:2374
- [57] Petrik P (2008) Ellipsometric models for vertically inhomogeneous composite structures. *Phys Stat Solidi A* 205:732
- [58] Salazar D, Soto-Molina R, Lizarraga-Medina EG, Felix MA, Radnev N, Marquez H (2016) Ellipsometric study of SiO_x thin films by thermal evaporation. *Open J Inorg Chem* 6:175
- [59] Nesheva D, Petrik P, Hristova-Vasileva T, Fogarassy Z, Kalas B, Šćepanović M, Kaschieva S, Dmitriev SN, Antonova K (2019) Changes in composite nc-Si-SiO₂ thin films caused by 20 MeV electron irradiation. *Nucl Instrum Methods Phys Res Sect B* 458:159–163
- [60] Xiong F, Li M-F, Malomo B, Yang L (2020) Microstructural evolution in amorphous-nanocrystalline ZrCu alloy under neutron irradiation. *Acta Mater* 182:18–28

Publisher's Note Springer Nature remains neutral with regard to jurisdictional claims in published maps and institutional affiliations.